25. ———, *J. Gen. Physiol.* **93**, 43 (1989).
26. E. Kopenhofer and H. Schmidt, *Pfluegers Arch.* **303**, 133 (1968).
27. G. K. Wang and G. Strichartz, *J. Gen. Physiol.* **86**, 739 (1985).
28. G. E. Kirsch, A. Skattebøl, L. Possani, A. M. Brown, *ibid.* **93**, 67 (1989).
29. F. J. Tejedor and W. A. Catterall, *Proc. Natl. Acad. Sci. U.S.A.* **85**, 8742 (1988).
30. C. D. Rasmussen, R. C. M. Simmen, E. A. MacDougall, A. R. Means, *Meth. Enzymol.* **139**, 642 (1987).
31. D. A. Melton, P. A. Kreig, M. R. Rebaliati, T. Maniatis, *Nucleic Acids Res.* **12**, 7035 (1984).
32. V. Glisin, R. Crkvenjakov, C. Byus, *Biochemistry* **13**, 2633 (1973).
33. W. A. Catterall, *J. Biol. Chem.* **251**, 5528 (1976).
34. We thank W. Newerly-Abranow for guidance and J. C. Roder for use of tissue-culture facilities and reagents. Supported by grants from the Medical Research Council of Canada and the Multiple Sclerosis Society of Canada to R.J.D., NIH research grants NS 15751 and NS 25704 to W.A.C., and a postdoctoral fellowship from the Multiple Sclerosis Society to J.O.

24 August 1989; accepted 20 November 1989

Subcellular Calcium Transients Visualized by Confocal Microscopy in a Voltage-Clamped Vertebrate Neuron

ARTURO HERNÁNDEZ-CRUZ,* FRANCISCO SALA,† PAUL R. ADAMS

Confocal laser-scanned microscopy and long-wavelength calcium (Ca^{2+}) indicators were combined to monitor both sustained and rapidly dissipating Ca^{2+} gradients in voltage-clamped sympathetic neurons isolated from the bullfrog. After a brief activation of voltage-dependent Ca^{2+} channels, Ca^{2+} spreads inwardly, and reaches the center of these spherical cells in about 300 milliseconds. Although the Ca^{2+} redistribution in the bulk of the cytosol could be accounted for with a radial diffusion model, local nonlinearities, suggesting either nonuniform Ca^{2+} entry or spatial buffering, could be seen. After electrical stimulation, Ca^{2+} signals in the nucleus were consistently larger and decayed more slowly than those in the cytosol. A similar behavior was observed when release of intracellular Ca^{2+} was induced by caffeine, suggesting that in both cases large responses originate from Ca^{2+} release sites near or within the nucleus. These results are consistent with an amplification mechanism involving Ca^{2+}-induced Ca^{2+} release, which could be relevant to activity-dependent, Ca^{2+}-regulated nuclear events.

THE SPATIAL DISTRIBUTION OF INTRACELLULAR Ca^{2+} after excitation in nerve cells depends on the location and density of Ca^{2+} channels, as well as buffering, sequestration, and release of Ca^{2+} within the cytoplasm. The dynamics of intracellular Ca^{2+} are relevant to the kinetics of Ca^{2+}-activated membrane conductances and other Ca^{2+}-regulated processes, such as transmitter release, release of intracellular Ca^{2+}, and activation of enzymes and genes (*1*). Time resolution in the order of milliseconds and spatial resolution in the micron range are required to monitor rapid local changes in the Ca^{2+} concentration ($[Ca^{2+}]$) associated with nerve excitation and to thus overcome the blurring effects of diffusion. We have used confocal microscopy to monitor the redistribution of the intracellular $[Ca^{2+}]$ ($[Ca^{2+}]_i$) after the entry of Ca^{2+} through voltage-gated Ca^{2+} channels and its release from caffeine-sensitive intracellular stores (*2*).

Confocal fluorescence microscopy has several advantages over conventional microscopy for Ca^{2+} imaging (*3*). (i) The narrower depth of field allows better visualization of intracellular details by eliminating out-of-focus signals. (ii) A substantially improved lateral spatial resolution is expected. (iii) Measurement errors due to path-length variations are minimized because a small and relatively constant volume of the cell is sampled throughout the focal plane. This last feature is particularly relevant, because currently available long-wavelength Ca^{2+} indicators are not suitable for the determination of absolute Ca^{2+} concentrations by ratio imaging (*4, 5*).

We measured the $[Ca^{2+}]_i$ of dissociated bullfrog sympathetic neurons under voltage-clamp conditions so as to allow precise control of transmembrane Ca^{2+} influx. The Ca^{2+} indicator fluo-3 (*4*) was used to monitor changes in $[Ca^{2+}]_i$. We rountinely used two image acquisition modes. In the frame-scanning mode (FSM), an image frame can be collected in 1 s. Steady or slowly changing gradients throughout the cell were monitored with this method. In the line-scanning mode (LSM), the monitored region of the cell was reduced to a narrow "slot" by scanning the beam in only one spatial dimension. Because of the small number of pixels acquired per cycle (384 in most cases), a temporal resolution of 5 ms or less was achieved, without the loss of spatial resolution. LSM images contain detailed spatiotemporal information of the changes in $[Ca^{2+}]_i$ that occur during the formation of the image. Thus, the changes in $[Ca^{2+}]$ across the cell (horizontal axis) can be followed as a function of time (vertical axis).

In the example shown in Fig. 1, a brief Ca^{2+} current produced an inward "wave" of increased $[Ca^{2+}]$ that reached the center of the cell in ~300 ms. Subsequently, $[Ca^{2+}]$ equilibrated across the cell, returning to resting values within 6 to 8 s. Although the $[Ca^{2+}]$ transients in the periphery were faster and larger than those at the center of the cell (Fig. 1, G and H), those near the cell membrane, although rapid, were attenuated because of cell curvature. Both Ca^{2+} transients and Ca^{2+} currents were absent in Ca^{2+}-free external solution or after superfusion with 100 μM Cd^{2+}. These observations represent, to our knowledge, the first experimental confirmation of the stimulus-induced, rapidly dissipating spatial Ca^{2+} gradients in the cytoplasm that had been previously modeled theoretically (*6*).

The basic features of Ca^{2+} dynamics after a brief period of Ca^{2+} entry could be mimicked with a diffusion model (*7*). Our formulation differs from previous radial diffusion models (*6*) in that it includes both mobile and stationary Ca^{2+} buffers (one of the mobile buffers being the dye itself), as well as a Ca^{2+} extrusion mechanism (*8*). Peripheral Ca^{2+} transients decay in two phases: an early phase, lasting about 300 ms and due mainly to diffusional redistribution across the cell, and a late phase, lasting for seconds and reflecting slow buffering and membrane extrusion. Spatial gradients across the cell are absent during the late phase. Under our experimental conditions and on the time scale of interest, fluo-3 seems to be the dominant fast Ca^{2+} buffer. The model predicts that the early phase would be slower and the late phase would be more rapid in the absence of dye; this follows from the Ca^{2+}-transporting properties of the diffusible exogenous buffer. Also, Ca^{2+} transients should be considerably larger throughout the cell in the absence of dye. A complex interplay between mobility, capacity, and affinity of intracellular buffers determines the time course, magnitude, and spreading of Ca^{2+} signals in the cytoplasm (*7*).

Howard Hughes Medical Institute, Department of Neurobiology and Behavior, State University of New York at Stony Brook, Stony Brook, NY 11794.

*To whom correspondence should be addressed at Department of Neurosciences, Roche Institute of Molecular Biology, Nutley, NJ 07110.
†Present address: Departamento de Neuroquímica, Universidad de Alicante, Alicante, Spain.

The magnitude of Ca^{2+} transients varied from cell to cell and did not always correlate with the size of the Ca^{2+} current. This may reflect differences in intrinsic fast buffering capacity or initial $[Ca^{2+}]_i$. Also, deviations from a symmetrical radial diffusion pattern were occasionally observed (Fig. 2). The larger Ca^{2+} signal on the left side of the pattern shown in Fig. 2F could result from inhomogeneities in Ca^{2+}-channel density (*9*) or intrinsic Ca^{2+} buffering (*10*) or both (compare Fig. 1A). A deviation of the stimulus-initiated Ca^{2+} redistribution from that predicted by the model was invariably seen when the scanning line transected the nucleus (Fig. 2B). The profile of $[Ca^{2+}]_i$ initially resembled the symmetric pattern shown in Fig. 1A, but then became markedly asymmetric, as the nuclear signal continued to rise while elsewhere $[Ca^{2+}]_i$ returned to basal values. In this example, the nuclear $[Ca^{2+}]$ increased by 140 n*M*, compared to 100 n*M* in the cytosol (*11*). Also, the nuclear $[Ca^{2+}]$ peaked about 600 ms later than a symmetrically located region in the cytosol and decayed more slowly (Fig. 2D).

It has been suggested that increases in $[Ca^{2+}]_i$ that outlast electrical stimulation may result from Ca^{2}-induced Ca^{2+} release from intracellular reservoirs (*12, 13*). Thus, the large nuclear signals might reflect Ca^{2+} release near or within this structure. To test this hypothesis, we examined the changes in the distribution of $[Ca^{2+}]_i$ produced by caffeine, a promoter of Ca^{2+}-induced Ca^{2+} release (*12–16*). For these experiments, a normal pipette solution was used (see legend to Fig. 3), to allow the recording of Ca^{2+}-activated membrane currents as an independent indicator of submembrane changes in $[Ca^{2+}]$. FSM images showed that caffeine produced a rise in $[Ca^{2+}]$ throughout the cell (Fig. 3, A through C). The nucleus, however, showed a considerably larger change. A ratio image obtained by dividing the image in Fig. 3B by that in Fig. 3A gave values of 1.49 ± 0.018 and 1.33 ± 0.017 for nucleus and cytosol, respectively (mean ± SD for six independent measurements over a .25 μm^2 area; $P < 0.001$). Nuclear $[Ca^{2+}]$ increased by an estimated 210 n*M* in Fig. 3B. These changes coincided with the development of a transient outward current (record not shown). LSM patterns including the nuclear region were produced to monitor Ca^{2+} movements during the release process. A sustained, rapid application of 10 m*M* caffeine produced a transient increase in $[Ca^{2+}]$, which peaked in about 1.5 s and was followed by a smaller, sustained plateau (Fig. 3D and 3F, upper panel). Several structures participated in the response, but the nuclear signal was again the most prominent (*17*).

It has been suggested that subsurface cisternae, a class of smooth endoplasmic reticu-

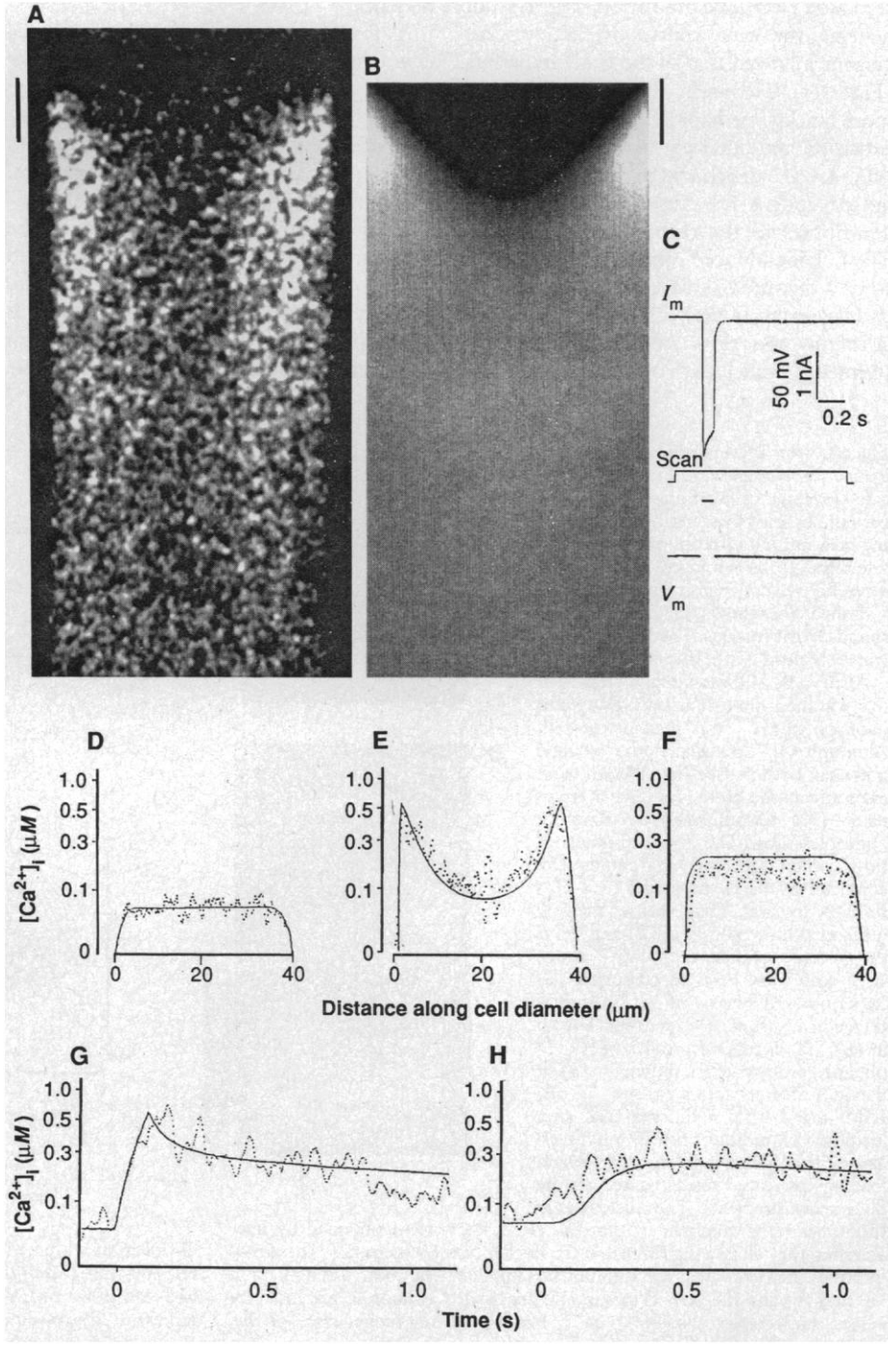

Fig. 1. (**A**) Dynamics of radial spread of Ca^{2+} monitored along the diameter of a sympathetic neuron. In LSM patterns, consecutive lines are plotted from top to bottom. The first few lines were acquired with the cell held at −70 mV. Then, a maximal inward current was evoked with a 100-ms step to +10 mV. A 10% transmission neutral-density filter was used to reduce laser intensity. The image was gaussian-filtered with a half-height width of 1 pixel. (**B**) Simulated LSM pattern obtained with a radial diffusion model (*7*). Pixel intensities represent the concentration of the Ca^{2+}–buffer B complex (*8*). Vertical lines in (A) and (B) represent the duration of the voltage step. (**C**) From top to bottom: membrane current (I_m), scan duration, and membrane voltage (V_m) corresponding to the experiment shown in (A). (D through H) Calcium concentration profiles in the temporal (vertical) and spatial (horizontal) domains extracted from patterns A (dotted traces) and B (solid traces). (**D**) Resting spatial profile. (**E**) Spatial profile at the end of the voltage step. (**F**) Spatial profile 1 s after the stimulus onset. Distances in (D) through (F) were measured from the left edge of the cell. (**G** and **H**) Temporal profiles at 2.5 μm beneath the membrane and at the center of the cell, respectively. Cell diameter, 40 μm. The pipette contained: 90 m*M* CsCl, 20 m*M* tetraethylammonium chloride, 5 m*M* Hepes-CsOH (*p*H 7.15), 1 m*M* adenosine triphosphate (ATP) (Mg^{2+} salt), and 100 μ*M* fluo-3.

lum, could be responsible for Ca^{2+} release and sequestration in vertebrate neurons (*18*). However, our data indicate that in response to caffeine, Ca^{2+} is released from peripheral locations as well as near the center of the cell (Fig. 3, D, E, and G). The earliest intracellular Ca^{2+} release after a brief (20- to 1000-ms) caffeine application is apparent in the region where the caffeine first reaches the cell (Fig. 3G, arrowhead). The release process then propagates throughout the cell, reaching the opposite location within 0.6 to 3 s [(*19*); compare response latencies in traces e and a of Fig. 3H]. These patterns are in marked contrast to the symmetrical, radial spread of Ca^{2+} seen after electrical stimulation (Fig. 1A). In general, the time course of the outward current followed that of the Ca^{2+} transients (Fig. 3H). However, the current decayed more quickly, perhaps because of faster Ca^{2+} extrusion and buffering near the membrane (*10*). A Ca^{2+}-dependent inhibition of a voltage-dependent K^+ current termed I_M also contributes to the current decay (*20, 21*). The caffeine-induced outward current seems to be a mixture of two Ca^{2+}-dependent K^+ conductances underlying fast spike repolarization and slow afterhyperpolarization (termed I_C and I_{AHP}, respectively), because it decreases, but does not disappear at holding potentials at which I_C should not be present (*22*).

We were unable to reproduce the repeated oscillations in $[Ca^{2+}]_i$ that have been observed by others in the presence of caffeine and high K^+ (*12, 15*). Possibly, dialysis during whole-cell recording perturbed the balance between the different processes underlying the oscillatory response (*23*). However, a brief (5 s or less) application of caffeine often produced a short-lived Ca^{2+} transient that was followed by a rebound rise in $[Ca^{2+}]$ (Fig. 3, E and F, lower panel), suggesting that some components involved in the oscillatory Ca^{2+} responses were still present.

As for the source of nuclear Ca^{2+} signals, it is conceivable that they originate either from a perinuclear organelle or from the nuclear envelope itself. However, the patterns of Ca^{2+} rise in the nucleus examined so far are not consistent with a peripheral origin of Ca^{2+}; rather, they suggest a simultaneous release throughout this structure (compare in Fig. 3F latencies of responses in traces 1 and 3, obtained from extreme positions within the nucleus). We feel it is premature to draw any conclusions from these results on the source of nuclear Ca^{2+}.

A differential regulation of nuclear $[Ca^{2+}]$ was not previously observed in bullfrog neurons (*12, 13*). This discrepancy could be due to the better discrimination of intracellular structures achieved with confocal microscopy. In support of our observations, recent studies have shown inositol 1,4,5-trisphosphate (IP_3)–receptor sites, IP_3-sensitive Ca^{2+} pools, and Ca^{2+}-dependent adenosine triphosphatase (Ca^{2+}-ATPase)–like proteins localized to perinuclear organelles and the nuclear envelope (*24, 25*). In addition, agonist-induced Ca^{2+} rises localized to the nuclear region have been reported in adrenal chromaffin cells (*25*).

According to our model, intracellular Ca^{2+} diffusion in whole-cell experiments is dominated by the contribution of the mobile exogenous buffer used to monitor $[Ca^{2+}]_i$. As most other models required, in addition to the exogenous Ca^{2+} indicator, a fast, high-capacity cytoplasmic buffer to account for stimulus-induced Ca^{2+} signals, our results suggest that some of the endogenous Ca^{2+} buffers of the cell (presumably soluble constituents) are rapidly lost by dialysis of the cell contents. This constitutes a major limitation of this technique. Under more physiological conditions, the contribution of the endogenous fast buffers

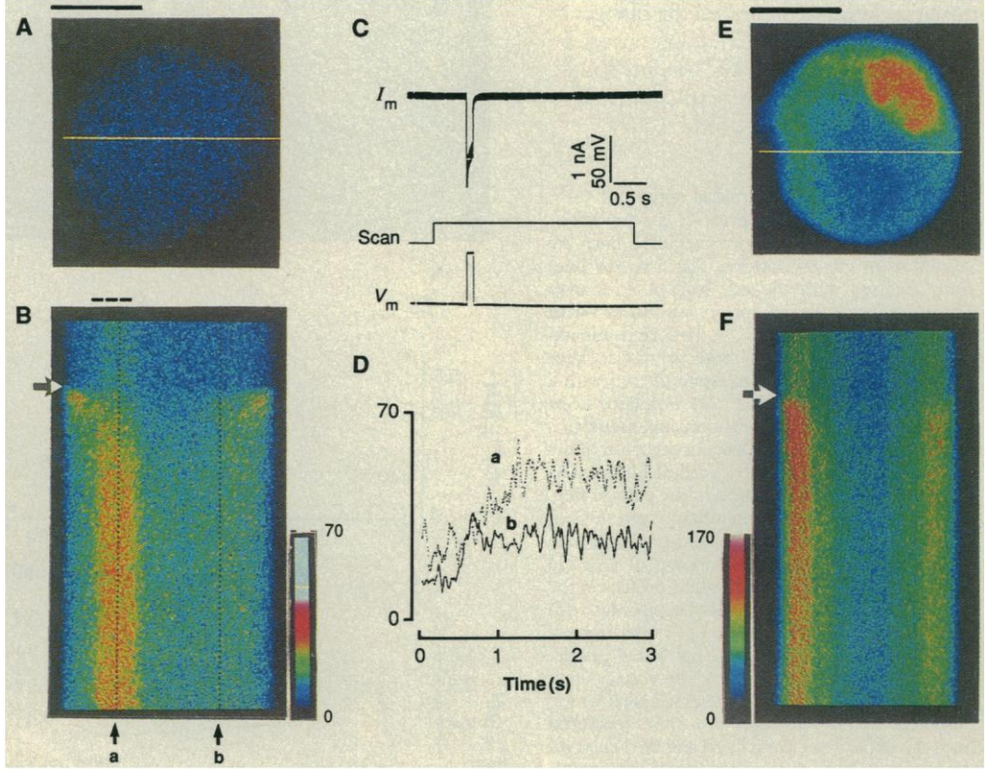

Fig. 2. (**A**) FSM image from a cell loaded for 10 min with fluorescent indicator (average of five frames). (**B**) LSM pattern obtained by scanning the beam at the position indicated by the horizontal line through the cell in (A). The slightly more fluorescent region (indicated with a dashed line above the image) corresponds to the nucleus. The first 100 lines were obtained with the cell resting at −70 mV. A 100-ms voltage step to 0 mV was then applied (arrow). Entry and diffusion of Ca^{2+} was then monitored. Although Ca^{2+} transients after a single pulse can be seen (see Fig. 1A), in most experiments the beam was further attenuated (3% transmission) to minimize photobleaching. The signal-to-noise ratio was then improved by averaging five consecutive images, separated by a 60-s recovery interval. Thus, each of the 500 horizontal lines plotted in (B) and (F) is the average of five consecutive scans. Each scan took ~3 s to complete. (**C**) Superimposed sweeps of I_m, scan duration, and V_m from the experiment shown in (B). (**D**) Temporal profiles of $[Ca^{2+}]$ obtained from pattern shown in (B) at the indicated locations (a and b). (**E**) FSM image from a different cell after loading with indicator for 20 min (average of five frames). In general, longer loadings produced more marked resting fluorescence gradients. The nucleus is in the upper right quadrant of the cell. (**F**) LSM pattern obtained by line-scanning the cell in a region below the nucleus, as shown in (E). The arrow indicates the time when the stimulus was applied. The color coding bars in (B) and (F) and the vertical axis in (D) are labeled as fluorescence intensity values, rather than absolute $[Ca^{2+}]$, because of inhomogeneities of dye distribution within the cell. Were the dye evenly distributed, values of 30, 50, 100, and 150 in these scales would represent $[Ca^{2+}]_i$ values of 82, 158, 515 and 2000 n*M*, respectively. Scale bars above images in (A) and (E) represent 20 μm. Pipette solutions were as in Fig. 1.

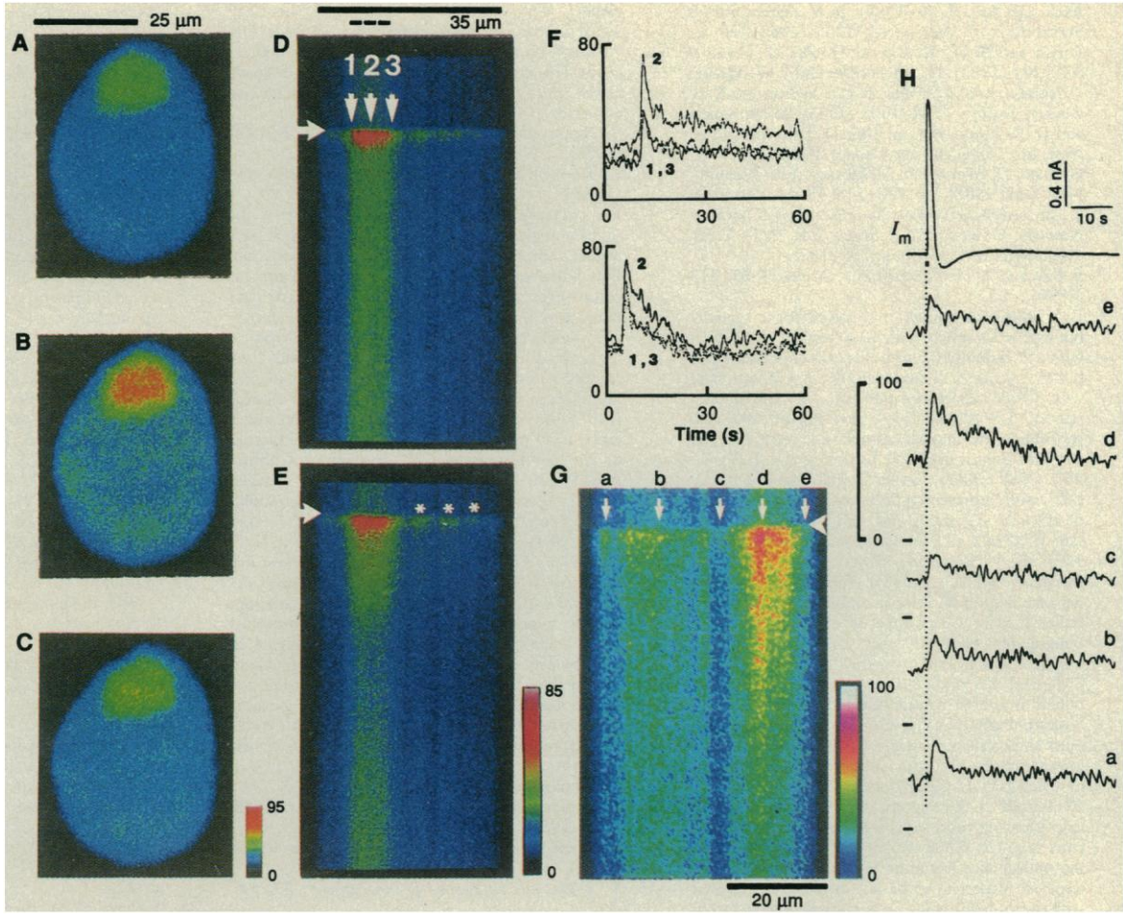

Fig. 3. (A to C) FSM images of a caffeine-induced Ca^{2+} release in a cell loaded for 15 min with fluo-3. (Each image, representing the average of six frames, took 6 s to complete.) (**A**) Fluorescence image at rest. (**B**) Image obtained at the start of caffeine application. (**C**) Image taken 5 min later. Caffeine (10 m*M*) was applied for 2.8 s with a puffer pipette positioned ≤100 μm from the left side of the cell. (**D** and **E**) LSM patterns of responses obtained from a different cell. These patterns took 62 s to complete. Noise was filtered as described in Fig. 1. The solid line above the images represents the extent of the cell diameter. A dashed line indicates the position of the nucleus. (D) Caffeine was puffed continuously, starting when indicated with the horizontal white arrow. (E) After a 10-min wash, caffeine was reapplied, but this time for only 5 s. Asterisks indicate presumptive release sites in the cytoplasm. Cell regions exhibiting smaller changes could represent areas of diffusional restriction or strongly buffered domains. (**F**) (upper and lower panels) Temporal profiles of $[Ca^{2+}]$ obtained at positions 1, 2, and 3 (center and edges of the nucleus) from the patterns shown in (D) and (E), respectively. Notice the delayed "rebound" response in (E) and (F), lower panel). (**G**) Response from a different cell to a 600-ms caffeine application. (**H**) Membrane current record (I_m) (holding potential, −30 mV) and Ca^{2+} transients (a to e) from the experiment shown in (G). Transients were taken at the positions indicated in (G). Small horizontal lines indicate 0 reference value. Position d corresponds to the center of the nucleus. The delay in peak latencies between traces e and a is 750 ms. Color-coding bars as in Fig. 2. Pipette contained: 90 m*M* potassium aspartate, 20 m*M* KCl, 1 m*M* ATP (Mg^{2+} salt), 5 m*M* Hepes-NaOH (*p*H 7.15), and either 0.1 m*M* (A to C) or 0.2 m*M* (D to H) fluo-3.

should be more important.

It has been suggested that in smooth muscle cells, the nucleus is screened from fluctuations in cytoplasmic $[Ca^{2+}]$ (*26*). Nuclear calcium also seems to be independently regulated in frog sympathetic neurons, but in the opposite fashion. Not only is the nucleus exposed to perturbations in cytosolic $[Ca^{2+}]$, but a local amplification of this signal seems to occur. This mechanism could give rise to large and prolonged increases in nuclear $[Ca^{2+}]$ after periods of sustained electrical activity, with minimal disturbance of cytosolic Ca^{2+} concentration. Our findings may be relevant to the proposed role of intranuclear Ca^{2+} in the signal transduction pathway linking neuronal stimulation to long-term structural and functional modifications of nerve cells (*27*).

Note added in proof: The main observations of this report, including the nuclear Ca^{2+} signal, have been confirmed in fura-2–loaded neurons isolated from the amphibian dorsal root ganglion (*28*).

REFERENCES AND NOTES

1. H. Rasmussen and P. Q. Barrett, *Physiol. Rev.* **64**, 939 (1984); R. S. Zucker and A. L. Fogelson, *Proc. Natl. Acad. Sci. U.S.A.* **83**, 3032 (1986); M. B. Kennedy, *Trends Neurosci.* **12**, 417 (1989).
2. Whole-cell patch-clamp recordings [O. P. Hamill, A. Marty, E. Neher, B. Sakmann, F. J. Sigworth, *Pfluegers Arch.* **391**, 85 (1984)] were obtained from dissociated bullfrog sympathetic ganglion neurons, as prepared by S. W. Kuffler and T. J. Sejnowski [*J. Physiol. (London)* **341**, 257 (1983)]. The $[Ca^{2+}]$ was monitored with membrane-impermeable fluo-3 (Molecular Probes, Eugene, OR). Electrode resistances ranged from 1 to 4 megohms with the internal solutions used. The external solution contained 108 m*M* NaCl, 3 m*M* KCl, 1 m*M* $NaHCO_3$, 0.5 m*M* NaH_2PO_4, 0.5 m*M* $MgCl_2$, 0.5 m*M* $MgSO_4$, 2 m*M* $CaCl_2$, 1 m*M* sodium pyruvate, 16 m*M* D-glucose, 2 m*M* Hepes-NaOH (*p*H 7.3), and 1 μ*M* tetrodotoxin. We assumed that the intracellular dye concentration reached equilibrium 10 min after a complete blockade of outward K^+ currents was observed. Fluorescence images were obtained with a laser-scanned confocal microscope (Lasersharp MRC-500, Bio-Rad) equipped with an argon ion laser and a fluorescein filter cartridge. Scanner and detectors were attached to a Zeiss IM-35 inverted microscope (water immersion, 0.75 numerical aperture, 40× objective). Illumination was limited to the periods of image acquisition. Confocal pinhole aperture settings were kept constant throughout the experiments. The detector output was fed into a frame store, and 384 by 512 pixel images were digitized to 8 bits and stored on magnetic media. Further image analysis was conducted on a SUN workstation (Sun Microsystems, Mountain View, CA). For in vitro calibration, we focused the microscope on 10-μl droplets of internal solution containing mixtures of Cs^+ and EGTA with and without Ca^{2+}, with a $[Ca^{2+}]$ between 10 n*M* and 10 μ*M*, calculated according to A. Fabiato and F. Fabiato [*J. Physiol. (Paris)* **75**, 463 (1979)]. An apparent dissociation constant (K_d) of fluo-3 for Ca^{2+} of 420 n*M* was obtained by this method.
3. T. Wilson and C. Sheppard, *Theory and Practice of Scanning Optical Microscopy* (Academic Press, New York, 1984); T. Wilson, *Ann. N.Y. Acad. Sci.* **483**, 416 (1986); G. J. Brakenhoff, H. T. M. Van der Voort, E. A. Van Spronsen, N. Nanninga, *ibid.*, p. 405; T. Wilson and A. R. Carlini, *J. Microsc.* **149**, 51 (1988); A. Fine, W. B. Amos, R. M. Durmin, P. A. McNaughton, *Trends Neurosci.* **11**, 346 (1988).
4. A. Minta, A. T. Harootunian, J. P. Y. Kao, R. Y. Tsien, *J. Cell Biol.* **105**, 9 (abstr.) (1987); A. Minta, J. Y. P. Kao, R. Y. Tsien, *J. Biol. Chem.* **264**, 8171 (1989); J. P. Y. Kao, A. Harootunian, R. Y. Tsien, *ibid.*, p. 8179.
5. R. Y. Tsien, *Trends Neurosci.* **11**, 419 (1988); *Annu. Rev. Neurosci.* **12**, 227 (1989).
6. M. P. Blaustein and A. L. Hodgkin, *J. Physiol. (London)* **200**, 497 (1969); P. F. Baker, A. L. Hodgkin, E. B. Ridgway, *ibid.* **218**, 709 (1971); M. C. Andresen, A. M. Brown, S. Yasui, *ibid.* **287**, 283 (1979); S. J. Smith and R. S. Zucker, *ibid.* **300**, 167 (1980); J. A. Connor and G. Nikolakopoulou, *Lect.*

Math. Life Sci. **15**, 79 (1982); R. S. Zucker and N. Stockbridge, *J. Neurosci.* **3**, 1263 (1983); M. E. Barish and S. H. Thompson, *J. Physiol. (London)* **337**, 201 (1983); N. Stockbridge and J. W. Moore, *J. Neurosci.* **4**, 803 (1984); A. L. Fogelson and R. S. Zucker, *Biophys. J.* **48**, 1003 (1985); S. M. Simon and R. R. Llinás, *ibid.*, p. 485; D. Tillotson and E. Nasi, in *Calcium and Ion Channel Modulation*, A. D. Grinnell, D. Armstrong, M. Jackson, Eds. (Plenum, New York, 1988), pp. 133–146; W. M. Yamada *et al.*, in *Methods in Neuronal Modeling: From Synapses to Networks*, C. Koch and I. Segev, Eds. (MIT Press, Cambridge, MA, 1989), pp. 97–135.

7. F. Sala and A. Hernández-Cruz, *Biophys. J.* **57**, 313 (1990).
8. Equations were numerically solved for a spatially homogeneous sphere with 40 concentric shells, each with a thickness of 0.5 μm. All shells contained three buffer systems, A, B, and C. Buffer A was stationary with a total capacity of 600 μ*M*, forward binding rate of 5×10^4 M^{-1} s^{-1}, and K_d of 400 n*M*, resembling the smooth endoplasmic reticulum [H. Rasgado-Flores, and M. P. Blaustein, *Am. J. Physiol.* **252**, C588 (1987)]. Buffer B, diffusible and kinetically faster, represented fluo-3, with a total capacity of 100 μ*M*, K_d of 420 n*M*, and a forward binding rate of $10^8 M^{-1}$ s^{-1}, similar to that of fura-2 [M. G. Klein, B. J. Simon, G. Szucs, M. F. Schneider, *Biophys. J.* **53**, 971 (1988)]. To better fit the data, we included an additional mobile and fast buffer, buffer C, with a total capacity of 20 μ*M*, forward binding rate of $10^8 M^{-1}$ s^{-1}, and K_d of 250 n*M*. Diffusion coefficients were 6×10^{-6} cm^2 s^{-1} for Ca^{2+} and 2.5×10^{-6} and 1×10^{-6} cm^2 s^{-1} for buffers B and C, respectively (either free or Ca^{2+}-bound). Initial $[Ca^{2+}]_i$ was 50 n*M*. At the outermost shell, calcium entry was modeled as a square inward current (2.5 nA, 100 ms) and pumping was modeled as by E. Gamble and C. Koch [*Science* **236**, 1311 (1987)]. A temporal step of 0.1 ms was used in computing most equations, but fast buffer systems required 0.005 ms for convergence. Because the optical slice has finite thickness, the LSM patterns are expected to be somewhat contaminated with out-of-focus light. To determine to what extent this could affect the pattern, we convolved the simulated (ideal) pattern assuming the very unfavorable case that all shells within 10 μm from the focal plane contributed to the signal. The contribution of unfocused shells was weighted according to their geometrical projections. The convolved pattern did not differ much from the ideal [that is, the peak $[Ca^{2+}]$ in Fig. 1G (solid trace) is underestimated by about 8% in the convolved pattern, and the rise in $[Ca^{2+}]$ in Fig. 1H (solid trace) occurs slightly earlier]. Very close to the membrane, the Ca^{2+} signal in the convolved pattern was considerably "diluted" because of the low background fluorescence. This explains our observation that the signals at the edges of the cell are smaller than otherwise expected.
9. S. Thompson and J. Coombs, *J. Neurosci.* **8**, 1923 (1988).
10. D. Tillotson and A. L. F. Gorman, *Nature* **286**, 816 (1980).
11. We calculated these values by assuming that the slightly higher nuclear fluorescence seen at rest results entirely from inhomogeneous dye distribution. [Alternatively, the dye bound to nucleoplasmic constituents could have an increased steady-state fluoresence intensity (*17*)]. Because of the characteristic nonlinear response of fluorescent Ca^{2+} indicators (*5*), the peak nuclear $[Ca^{2+}]$ would have reached 150 to 200 n*M* if the higher resting nuclear fluorescence were partially due to a higher nuclear $[Ca^{2+}]$ (see below). Nucleus to cytosol fluorescence ratios (n:c) ranged between 1.5 and 2.5. Exposure to the nonfluorescent Ca^{2+} ionophore 4-bromo A23187 (20 μ*M*) in the presence of 2 m*M* extracellular Ca^{2+}, which presumably suppresses intracellular Ca^{2+} gradients by causing massive Ca^{2+} entry [D. A. Williams, K. E. Fogarty, R. Y. Tsien, F. S. Fay, *Nature* **318**, 558 (1985)], did not suppress this fluorescence gradient, although the n:c ratio decreased by 20 to 50%. This suggests that although the dye is more concentrated (or more fluorescent) in the nucleus, a $[Ca^{2+}]$ gradient is also present. In the absence of a transmembrane Ca^{2+} gradient, exposure to 10 μ*M* digitonin, which disrupts the plasma membrane, caused the fluorescence gradient to dissipate within seconds, suggesting that the dye was not tightly bound to immobile structures in the nucleus.
12. D. Lipscombe *et al.*, *Neuron* **1**, 355 (1988).
13. D. Lipscombe *et al.*, *Proc. Natl. Acad. Sci. U.S.A.* **85**, 2398 (1988).
14. I. R. Neering and R. N. McBurney, *Nature* **309**, 158 (1984).
15. K. Kuba and S. Nishi, *J. Neurophysiol.* **39**, 547 (1976).
16. K. Kuba, *J. Physiol. (London)* **298**, 251 (1980).
17. We assume that fluo-3, like other dyes, is bound to some extent to soluble cytoplasmic constituents. If the higher nuclear fluorescence at rest indicates more abundant binding sites for fluo-3 in the karyoplasm, then the enhanced nuclear signals could be explained if bound fluo-3 had a lower dissociation constant (K_d) for Ca^{2+}. This, however, seems unlikely because binding to macromolecules increases the K_d of other Ca^{2+} indicators [R. Y. Tsien, T. J. Rink, M. Poenie, *Cell Calcium* **6**, 145 (1985)]. For instance, the K_d of fura-2 increases more than threefold by binding to aldolase, an abundant myoplasmic protein [M. Konishi, A. Olson, S. Hollingworth, S. M. Baylor, *Biophys. J.* **54**, 1089 (1988)]. A weaker Ca^{2+} buffering near the nucleus of invertebrate neurons has been inferred because Ca^{2+} injections at the center of the cell produce the largest Ca^{2+} signals (*10*). We tested whether such nonuniform spatial buffering could explain our observations. A nuclear region was defined in the core of the model cell, and its buffering capacity was either increased or decreased with respect to the cytosol. Neither situation reproduced the enhanced nuclear responses observed in bullfrog sympathetic neurons. Most likely, the nucleus would be well buffered in our study, because of its apparent higher affinity to bind fluo-3.
18. M. Henkart, *Fed. Proc. Fed. Am. Soc. Exp. Biol.* **39**, 2783 (1980); S. Fujimoto, K. Yamamoto, K. Kuba, K. Morita, E. Kato, *Brain Res.* **202**, 21 (1980).
19. A. Hernández-Cruz, F. Sala, P. R. Adams, *Soc. Neurosci. Abstr.* **15**, 17 (1989).
20. P. J. Pfaffinger *et al.*, *Neuron* **1**, 477 (1988).
21. N. Akaike and J. Sadoshima, *J. Physiol. (London)* **412**, 22 (1989); N. V. Marrion *et al.*, *Soc. Neurosci. Abstr.* **15**, 16 (1989).
22. P. R. Adams, A. Constanti, D. A. Brown, R. B. Clark, *Nature* **296**, 746 (1982); D. A. Brown, A. Constanti, P. R. Adams, *Cell Calcium* **4**, 407 (1983); P. Pennefather, B. Lancaster, P. R. Adams, R. A. Nicoll, *Proc. Natl. Acad. Sci. U.S.A.* **82**, 3040 (1985).
23. K. Kuba and S. Takeshita, *J. Theor. Biol.* **93**, 1009 (1981).
24. C. A. Ross *et al.*, *Soc. Neurosci. Abstr.* **15**, 657 (1989); A. Verma, C. A. Ross, S. Supattapone, D. Verma, S. H. Snyder, *ibid.*, p. 658.
25. R. D. Burgoyne *et al.*, *Nature* **342**, 72 (1989).
26. D. A. Williams *et al.*, *Science* **235**, 1644 (1987).
27. J. I. Morgan and T. Curran, *Nature* **322**, 552 (1986); in *Cell Calcium Metabolism*, G. Fiskum, Ed. (Plenum, New York, 1989), pp. 305–312; *Cell Calcium* **9**, 303 (1989); *Trends Neurosci.* **12**, 459 (1989).
28. A Hernández-Cruz and J. A. Connor, unpublished results.
29. We thank J. A. Connor, R. Horn, and N. V. Marrion for comments on the manuscript; M. González for help with spectrofluorometric measurements; C. C. Choudhari for computer programming; and B. Burbach for technical assistance. F.S. was supported by Fundación Juan March (Spain). Supported in part by NIH grant NS1857906.

31 August 1989; accepted 11 December 1989